In Silico Evaluation of YCT-529:

Pharmacokinetics, ADME Properties, and Clinical Implications for Male Contraception

Capstone Project

Prof. Stan

Minerva University

April 5, 2025

Contents

Abstract

This study employs physiologically based pharmacokinetic (PBPK) modeling to characterize the pharmacokinetics of YCT-529, a non-hormonal male contraceptive, across diverse populations and dosing regimens. Using PK-Sim and ADMETLab 3.0, simulations were conducted in **4,000 participants** (1,000 each of Black Americans, East Asians, White Americans, and Europeans) at **four doses** (15 mg, 45 mg, 90 mg, and 180 mg). A control compound was also modeled, resulting in a total of **16,000 simulations**. Additionally, Atazanavir, a CYP3A4-metabolized reference drug, was simulated in **1,000 individuals** to validate the modeling approach.

YCT-529 exhibited rapid absorption, with $T_{\max}$ occurring within **1–3 hours** and dose-dependent increases in systemic exposure, reaching $C_{\max}$ values of **50 µg/L at 15 mg** and **500 µg/L at 180 mg**. East Asians demonstrated the highest systemic retention (**C_{max} 500 µg/L at 180 mg**), whereas Black Americans had the lowest (**300 µg/L**), consistent with known CYP3A4 metabolic variability. Dietary intake significantly influenced absorption, as fasting increased $C_{\max}$ to **100 µg/L**, while high-fat meals reduced it to **55 µg/L**. The significance of these differences, both statistically and practically, should be further explored to optimize dosing strategies. The predicted pharmacokinetics of Atazanavir closely mirrored clinical data, supporting the validity of the simulations. Limitations include reliance on computational models without experimental validation, necessitating further in vivo studies to refine dosing regimens and confirm findings. These results highlight the utility of PBPK modeling in optimizing contraceptive pharmacotherapy, guiding clinical trial design, and tailoring treatment strategies based on population-specific pharmacokinetics.

Keywords: YCT-529, pharmacokinetics, PBPK modeling, non-hormonal male contraceptive, PK-Sim, ADMETLab, population-specific pharmacokinetics, contraceptive pharmacotherapy, CYP3A4 metabolism

Introduction

Background

YCT-529 represents a significant advancement in the field of male contraceptives, offering a novel, non-hormonal mechanism of action. Unlike traditional hormonal contraceptives, which modulate the endocrine system and are often associated with adverse side effects, YCT-529 operates through a targeted, non-hormonal pathway. As noted in prior review, YCT-529 inhibits key biological processes essential for spermatogenesis, positioning it as a promising alternative for male contraception [32, 33]. However, understanding its pharmacokinetics - specifically how it behaves once administered - is critical for further clinical development.

Research Context

Research on YCT-529 remains limited due to proprietary restrictions on preclinical and clinical data. Despite its progression to clinical trials, comprehensive datasets on its ADME properties and pharmacokinetics remain unavailable until publication by *Communications Medicine*. This lack of empirical data hinders precise predictions regarding safety, efficacy, and dosing. As highlighted by Kimmelman et al. [21], computational modeling and theoretical frameworks become essential in addressing these knowledge gaps, enabling preliminary pharmacokinetic assessments. Without direct experimental validation, exploratory methodologies serve as a crucial tool for understanding YCT-529's metabolism, systemic distribution, and potential therapeutic applications.

In the absence of direct experimental data, alternative approaches become essential for informed discovery. Physiologically based pharmacokinetic (PBPK) models offer a powerful method to simulate YCT-529's behavior *in silico*, integrating molecular descriptors, physiological variables, and population-specific factors to predict pharmacokinetics. Tools like PK-Sim facilitate plasma concentration predictions and metabolic pathway identification, forming a basis for hypothesis generation. As Edginton et al. [13] demonstrated, PBPK models effectively address knowledge gaps in data-limited scenarios, making exploratory research critical for characterizing YCT-529's therapeutic profile and guiding confirmatory clinical studies.

Research Question

The research question, *How can computational pharmacokinetic modeling provide preliminary insights into the ADME properties of YCT-529?*, is critical for addressing knowledge gaps in YCT-529's pharmacokinetics without experimental data. Using computational tools such as SMILES generators, ADMETLab, and PK-Sim, this study simulates key

ADME processes to predict drug behavior. Comparisons with a placebo, microcrystalline cellulose (MCC), and Atazanavir as a validation reference provide essential context for absorption, distribution, and metabolism. These insights inform dosage optimization, predict drug interactions, and guide clinical trial designs, demonstrating the utility of computational pharmacokinetics in evaluating novel contraceptives.

Objectives

This study aims to analyze the pharmacokinetics of YCT-529 using computational models, addressing the lack of empirical data and providing preliminary ADME insights. The key objectives are:

- **Pharmacokinetic Modeling:** Simulate in-silico clinical trials using PK-Sim to predict YCT-529's bioavailability, dosage requirements, and metabolic pathways.
- **Comparative Analysis:** Evaluate YCT-529 against a placebo (microcrystalline cellulose) and Atazanavir to validate results and contextualize absorption, distribution, and metabolism.
- **Optimization and Validation:** Guide dosage planning, assess computational modeling limitations, and provide a foundation for future clinical studies.

Achieving these objectives advances the understanding of YCT-529's pharmacokinetics and its potential as a non-hormonal male contraceptive.

Methodology

I followed a structured computational workflow to simulate YCT-529's pharmacokinetics using PBPK modeling tools (see Figure ϕ). I generated the SMILES string, predicted physicochemical properties via ADMETLab [23], and modeled ADME behavior in PK-Sim [42]. To validate my results, I compared YCT-529 against microcrystalline cellulose (MCC) as a placebo [3, 38] and Atazanavir as a reference drug [2]. I selected PK-Sim over BioGears [8] due to its user-friendly interface, physiologically realistic models, and robust PBPK capabilities. This methodology allowed me to generate accurate pharmacokinetic predictions, analyze absorption, distribution, metabolism, and excretion, and establish a validated baseline through placebo and reference drug comparisons.

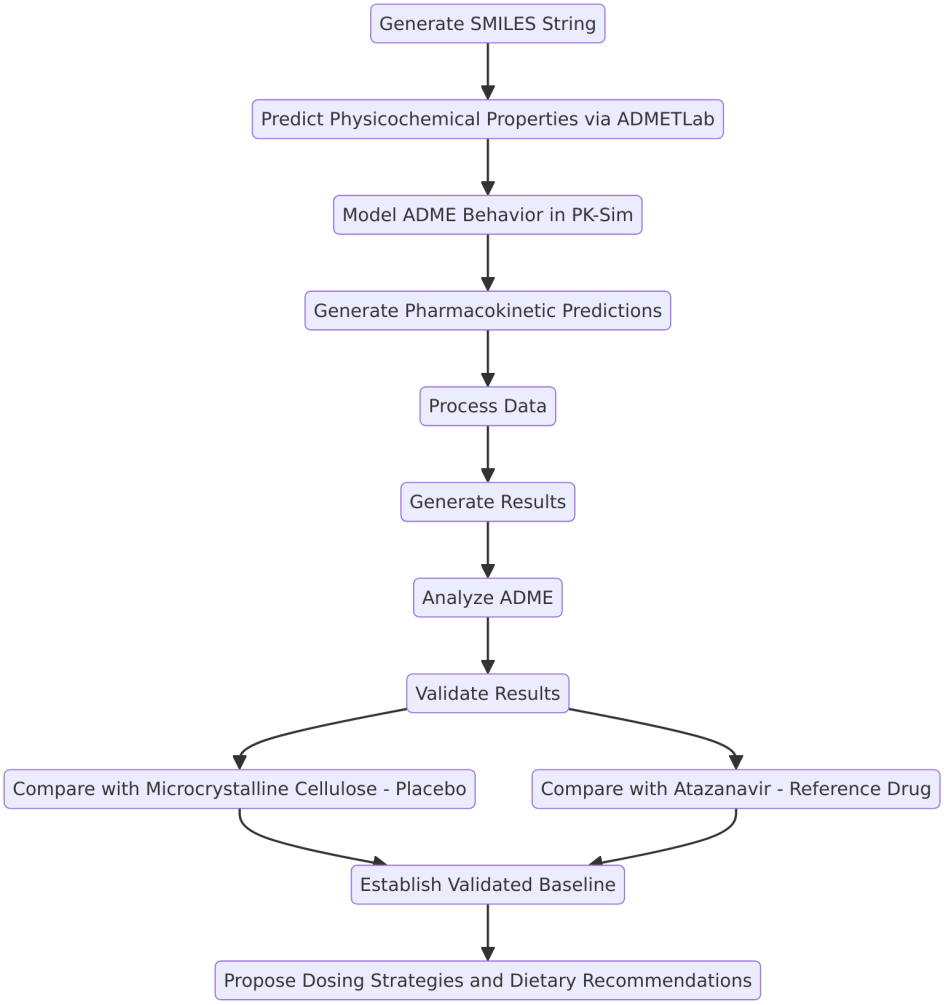

Figure ϕ: Sequential computational workflow for modeling YCT-529's pharmacokinetics. The workflow includes molecular structure generation, ADMET property prediction, PBPK modeling in PK-Sim, result analysis, and validation using a placebo (MCC) and a reference drug (Atazanavir).

SMILES String Generation

The first step in the computational workflow for analyzing YCT-529 involved using the SMILES generator available at Cheminfo.org [10]. I replicated the structure of YCT-529 with high precision referencing the molecular structure provided by the PubChem database [28].

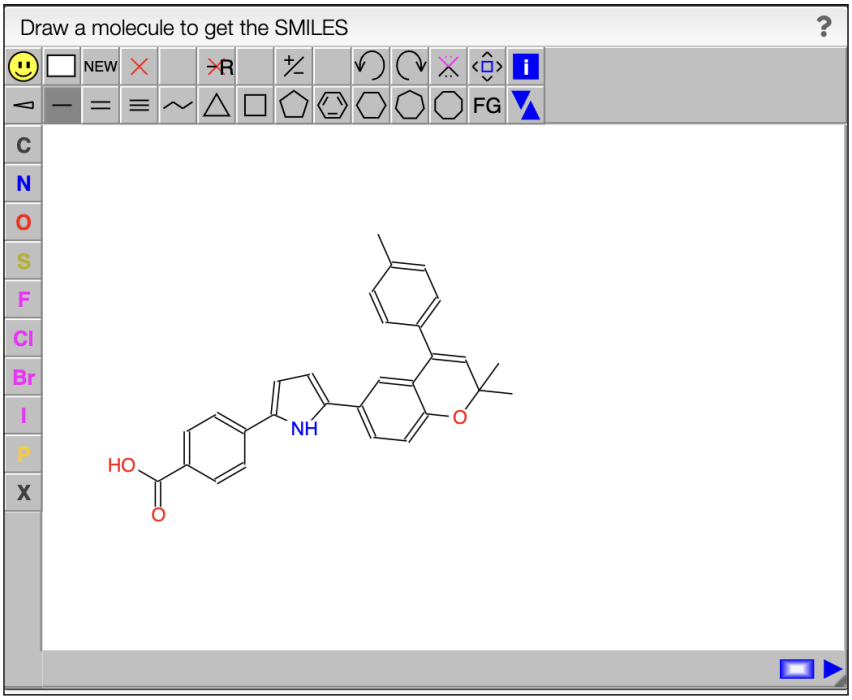

Figure 1: *Structure of YCT-529 constructed using the JSME molecular editor on Cheminfo.org for SMILES string generation, illustrating the compound's key functional groups and molecular framework [10].*

The SMILES string generated for YCT-529 was:
`Cc5ccc(C3=CC(C)(C)Oc4ccc(c2ccc(c1ccc(C(=O)O)cc1)[nH]2)cc34)cc5`.

I verified the SMILES string using ChemDraw to ensure accuracy. This standardized format is essential for cheminformatics tools like ADMETLab and PK-Sim. For MCC, I retrieved the D-glucose SMILES from PubChem [28], ensuring precision and facilitating its integration into subsequent computational analyses.

ADMETLab 3.0 Analysis

After generating the SMILES string for YCT-529, I analyzed the compound using ADMETLab 3.0, a cheminformatics platform that evaluates physicochemical, medicinal chemistry, ADME, and toxicity properties. The physicochemical properties, all enumerated in Appendix ϕ, included molecular weight (435.18 g/mol), LogP (5.706), LogS (-5.761), and TPSA (62.32 Å^2), alongside density (0.925 g/cm^3) and flexibility (0.138). The high LogP value of 5.706 suggests strong lipophilicity, enhancing membrane permeability but potentially limiting solubility [24]. This aligns with the LogS value of -5.761, corresponding to a solubility of approximately 0.067 mg/mL, which may hinder gastrointestinal dissolution. The TPSA of 62.32 Å^2 suggests moderate polarity, supporting passive diffusion while maintaining sufficient hydrophilicity for receptor binding. ADMETLab confirmed that YCT-529 adheres to Lipinski's Rule of Five, which evaluates molecular weight, hydrogen bond donors/acceptors, and lipophilicity. Compliance

with this rule indicates favorable absorption and permeability when administered orally [24]. However, the rejection of the GSK rule, which considers solubility and synthetic feasibility, suggests potential challenges in manufacturing and ADMET liabilities, such as toxicity risks [17]. This was reflected in toxicity predictions, which indicated high risks for drug-induced liver injury (DILI: 0.998) and genotoxicity (0.983). Despite these concerns, ADMETLab's machine-learning algorithms generate reliable predictions, supporting the exploratory nature of this research [44].

To establish a baseline comparison, I selected microcrystalline cellulose (MCC) as the placebo due to its well-documented inert and non-absorbable properties in pharmaceutical formulations [38, 3]. MCC is a polymer composed of glucose monomers, making it hydrophilic but non-ionizable, with an approximated LogP of 0. The molecular weight of MCC (180.06 g/mol) is equivalent to its monomeric unit, D-glucose, which has a LogP of -2.229, confirming its hydrophilic nature and inability to partition into lipid bilayers. The solubility of D-glucose (LogS 0.339) is significantly higher than MCC's near-insolubility (<0.01 g/L), reflecting the reduced water solubility caused by polymerization. Additionally, MCC exhibits negligible plasma protein binding or metabolic activity, making it pharmacologically inactive and ideal as a placebo for comparative pharmacokinetic modeling. These insights ensured MCC's accurate representation in PK-Sim, allowing for a meaningful evaluation of YCT-529's pharmacokinetic properties.

Building the Pharmacokinetic Model

I used PK-Sim (Version 12.0) to construct a physiologically based pharmacokinetic (PBPK) model for YCT-529, MCC, and Atazanavir. By integrating physicochemical and ADME data from ADMETLab, I simulated absorption, distribution, metabolism, and excretion across tissues. PK-Sim's Monte Carlo simulations enabled interindividual variability modeling, supporting population-level pharmacokinetic predictions [13].

PK-Sim Overview: Etymology, Function, and Applicability

PK-Sim bridges experimental data and in silico simulations using dynamic compartmental modeling across 18 tissues [42]. Its predictive capabilities for lipophilic drugs like YCT-529 are well-documented [30]. The software successfully models retinoic acid receptor antagonists, supporting its application to YCT-529 [31], with accuracy derived from clinical and preclinical physiological datasets.

Model Development

I created my model in PK-Sim in the following steps: Individuals and Populations, Compound Creation, and Formulation and Administration Protocols.

1. Individuals and Populations: I defined the demographic and physiological characteristics of simulation subjects to reflect clinical realities and scientific rationale. Using PK-Sim's race-specific models, I generated populations of 1000 Black American, East Asian, White American, and European males (ages 25–60, BMI 18–32 kg/m^2) for YCT-529, MCC, and Atazanavir, ensuring relevance to ongoing clinical trials (NCT06094283, NCT06542237). Ethnic differences in drug metabolism, particularly CYP2C19 and CYP2C8 polymorphisms in East Asians, influence systemic exposure and clearance [45]. Variations in enzyme expression and transporters among African and European populations further impact pharmacokinetics [41]. PK-Sim's population module randomized physiological parameters across 1000 individuals per group, generating 4000 total subjects, allowing robust inter-individual and inter-ethnic comparisons. Despite PK-Sim's limitations in modeling additional ethnic groups like africans, these populations provide a clinically grounded baseline for evaluating YCT-529's ADME properties.

2. Compound Creation: I constructed the YCT-529 model in PK-Sim by integrating key physicochemical and ADME properties. Lipophilicity, represented by a LogP of 5.706 and a $\text{LogD}_{7.4}$ of 3.356, was critical for modeling membrane permeability and tissue distribution [44, 6]. The solubility at pH 7.4 (0.29 g/L), derived from LogS (-5.761), was incorporated to reflect moderate solubility constraints. The fraction unbound (Fu = 0.537%) indicated strong plasma protein binding (98.8%), which significantly impacts distribution and clearance [33]. These parameters align with the Biopharmaceutics Drug Disposition Classification System (BDDCS), correlating lipophilicity and solubility with absorption profiles [6].

YCT-529's metabolism was primarily mediated by CYP3A4, with additional contributions from CYP2C8 and CYP2C9 for hydroxylation [40, 29]. Phase II metabolism involved glucuronidation (UGT1A1, UGT2B7) and sulfation (SULT1E1, SULT2A1), leading to renal and biliary excretion [40]. Atazanavir, metabolized by CYP3A4 and UGT1A1, served as a reference due to its similar metabolic pathways, high plasma protein binding (99%), and biliary excretion [40]. The integration of these metabolic pathways ensured that the PK-Sim model accurately represented YCT-529's pharmacokinetics, aligning with established drug metabolism principles.

3. MCC Compound Creation: The creation of the MCC model in PK-Sim was straightforward, as its physicochemical and ADME properties are well-documented in literature and pharmacopeias. MCC, a glucose polymer (PubChem CID: 5793), was assigned a molecular weight of 180.06 g/mol, accurately reflecting its monomer composition [38]. Its LogP was set to approximately 0, consistent with its hydrophilic nature and inability to partition into lipid bilayers [38]. A fraction unbound (Fu) of 1.0 was applied, as MCC does not bind plasma proteins or enter circulation [3]. With no ionizable groups,

pKa values were excluded, and solubility at physiological pH (7.4) was defined as <0.01 g/L, reflecting its practical insolubility [25]. The effective molecular weight remained 180.06 g/mol due to the absence of halogens or modifications [3]. I configured PK-Sim's compound creation module to represent MCC's non-absorbable, inert properties accurately. Intestinal permeability was set to <0.001 cm/s to reflect its lack of absorption, and volume of distribution (Vd) was omitted since MCC does not enter systemic circulation. No metabolic enzymes were assigned, as MCC resists enzymatic degradation in humans. Excretion was set as fecal, ensuring its pharmacokinetic profile as a placebo remained isolated from active pharmacological effects.

4. Atazanavir Compound Creation: I incorporated Atazanavir into my PK-Sim model by directly importing its pre-constructed compound file from the Open Systems Pharmacology Suite [2]. No modifications were made to its physicochemical or ADME parameters. Atazanavir, a lipophilic drug with a LogP of 2.12 and molecular weight of 704.9 g/mol, exhibits extensive plasma protein binding (Fu = 0.14) and undergoes primary metabolism via CYP3A4, as defined in its validated PBPK model [2]. Given its established metabolism, renal excretion accounts for approximately 7% of elimination, with the remainder undergoing biliary excretion [2]. Its inclusion provides a pharmacokinetic reference for YCT-529's metabolic behavior, particularly in assessing CYP3A4-mediated metabolism and biliary clearance.

5. Formulation and Administration Protocols: I defined dosing regimens based on clinical trials evaluating single and repeat ascending oral doses of YCT-529 (NCT06094283, NCT06542237). YCT-529 was administered orally at 15 mg, 45 mg, 90 mg, and 180 mg, dissolved in simulated gastric fluid, ensuring uniform delivery across all populations. Each dose was tested across 1000 Black American, East Asian, White American, and European males, resulting in 16 simulations (4 races $\times$ 4 doses). Similarly, microcrystalline cellulose (MCC) was administered at identical doses in simulated gastric fluid as a placebo to isolate the pharmacokinetic effects of YCT-529, leading to an additional 16 simulations. All simulations were conducted under a light meal dietary condition to ensure consistency in absorption parameters. For Atazanavir, I implemented a single-dose 400 mg oral capsule regimen across the same population (1000 individuals per race) using PK-Sim's predefined compound file [2]. This allowed comparative pharmacokinetic profiling, particularly in evaluating CYP3A4-mediated metabolism and biliary excretion. I configured PK-Sim to simulate each dosing scenario, capturing pharmacokinetic parameters such as C_{max}, T_{max}, and AUC for YCT-529, MCC, and Atazanavir. The results were exported to Google Spreadsheets for aggregation and further analysis. This methodology, while robust, could be enhanced by expanding the placebo group to refine interindividual variability and baseline pharmacokinetics further.

Model Analysis

Blood plasma concentration (C_p), specifically venous plasma concentration, is a key pharmacokinetic (PK) parameter that quantifies the amount of drug present in plasma at a given time. PK-Sim models venous rather than arterial plasma concentrations because venous blood represents post-capillary circulation, reflecting the net effect of absorption, distribution, metabolism, and excretion (ADME). Unlike arterial plasma, which reflects immediate systemic distribution post-cardiac output, venous plasma better approximates drug availability to tissues after metabolic processing and first-pass effects [16]. Venous sampling is also more practical and commonly used in clinical PK studies, allowing for direct comparison with experimental datasets. Two essential PK metrics derived from venous C_p are the maximum concentration (C_{max}) and the time to reach C_{max} (T_{max}). While C_{max} is typically in µmol/L, I measured it in µg/L to reflect mass-based systemic exposure, aiding dose-response comparisons and aligning with Atazanavir clinical data [2]. This metric influences both potency and safety, as excessively high values may indicate toxicity, while suboptimal peaks may suggest insufficient therapeutic efficacy. T_{max}, measured in hours, reflects absorption rate; shorter T_{max} values correspond to rapid absorption, whereas longer values indicate delayed release or slower uptake [26].

The relationship between venous C_p and other PK parameters, such as clearance (CL) and volume of distribution (V_d), follows the equation:

$$C_p = \left(\frac{\text{Dose}}{V_d}\right) \cdot e^{-\frac{CL}{V_d} \cdot t},$$

where t represents time. This equation highlights the impact of V_d on C_p; a higher V_d results in a lower C_p due to extensive tissue distribution, while a lower V_d confines the drug to plasma, yielding a higher C_p. Venous C_p profiles also inform bioavailability (F) and allow for area under the curve (AUC) calculations, which quantify systemic exposure over a given time, typically 24 hours [26]. Additionally, venous C_p refines dosing strategies by delineating therapeutic windows. Drugs with narrow safety margins require precise monitoring of C_{max} and C_{min} to maintain efficacy while preventing toxicity. The blood-to-plasma ratio (R_b) further refines venous C_p interpretation by accounting for drug partitioning into blood cells, offering insights into systemic distribution dynamics. By integrating venous C_p with AUC, CL, and V_d, PK modeling optimizes dosing regimens and enhances therapeutic predictions [16].

In summary, I integrated physiologically based pharmacokinetic modeling in PK-Sim, defining precise dosing regimens, metabolic pathways, and venous plasma concentration analysis. By validating assumptions with literature, optimizing simulations for YCT-529, MCC, and Atazanavir, and minimizing confounding factors, this methodology ensures

interpretable, reliable results that guide informed pharmacokinetic assessments and future research applications.

Results

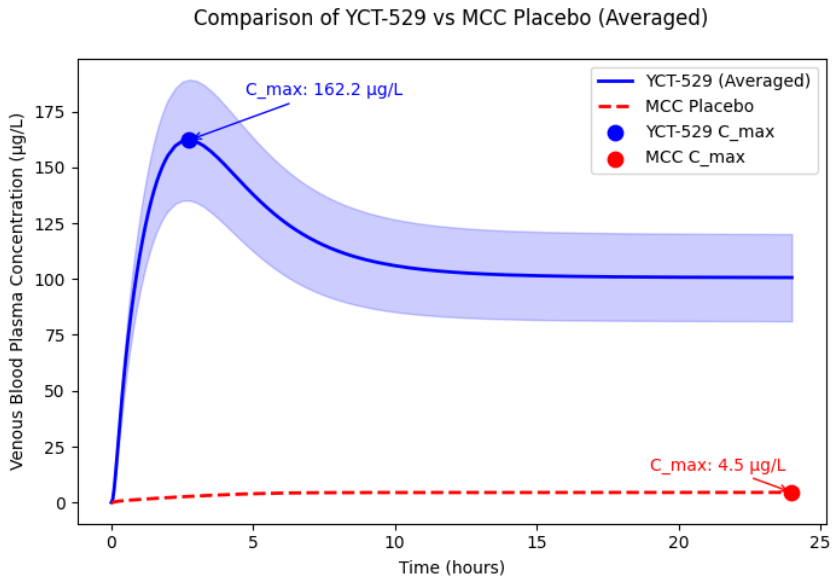

(a) Comparison of YCT-529 vs MCC Placebo (Averaged)

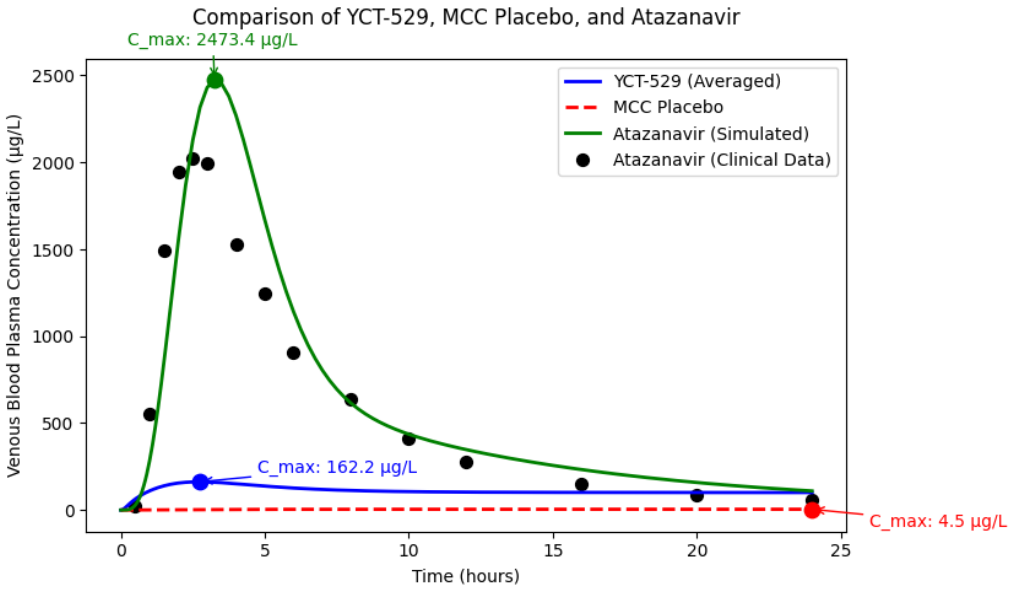

(b) Comparison of YCT-529, MCC Placebo, and Atazanavir

Figure 2: *Plasma concentration profiles for YCT-529, MCC placebo, and Atazanavir. (a) YCT-529 achieves a peak concentration (C_{max}) of approximately 0.5 µmol/L at 1 hour, while the MCC placebo remains below 0.02 µmol/L throughout 24 hours. (b) Atazanavir shows significantly higher peak concentrations compared to YCT-529 and MCC placebo, validating its pharmacokinetic model as a reference drug.*

I observed that YCT-529 plasma concentrations increased in a dose-dependent manner, with clear differences between active drug absorption and the placebo (MCC). **Figure 2, Panel A** shows that YCT-529 reached its peak concentration (C_{max}) rapidly, while the MCC placebo consistently remained below 10 µg/L across all time points, confirming minimal systemic absorption.

When I compared YCT-529 to Atazanavir, I found that the simulated pharmacokinetics for Atazanavir closely matched clinical data, reinforcing the validity of my computational model for predicting YCT-529's behavior. Atazanavir reached a much higher C_{max} (2500 µg/L) and exhibited rapid systemic clearance. Even at the highest dose (180 mg), YCT-529's C_{max} (353.9 µg/L) remained significantly lower than Atazanavir, indicating lower systemic exposure.

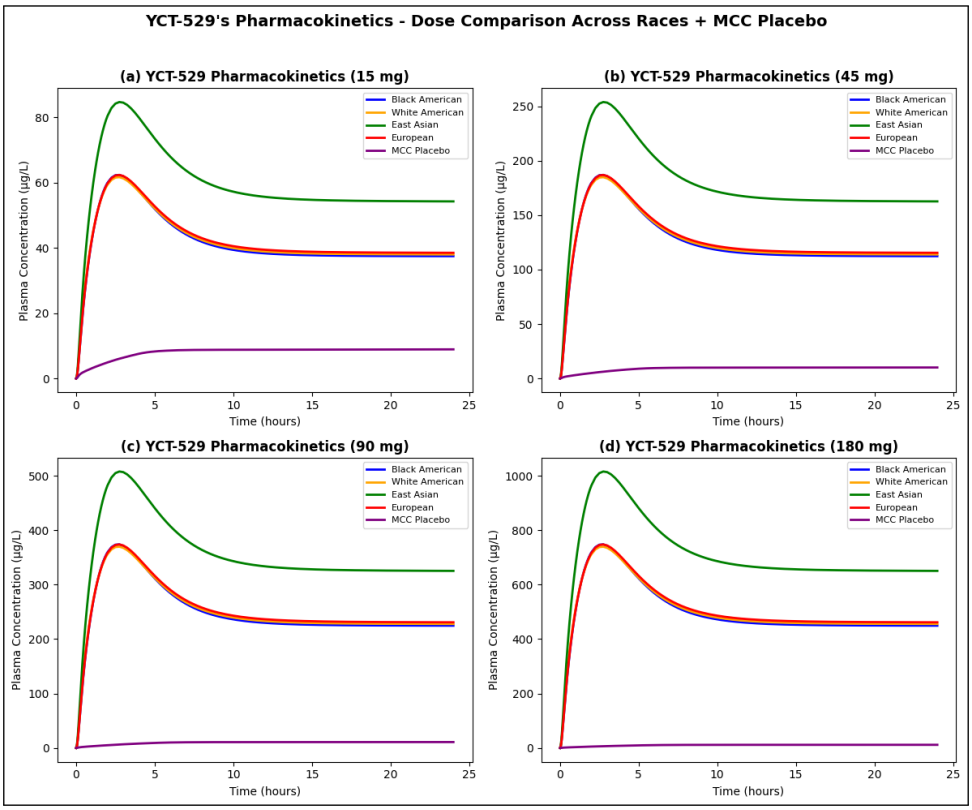

Figure 3: *Plasma concentration-time profiles for YCT-529 at 15 mg, 45 mg, 90 mg, and 180 mg doses across Black American, White American, East Asian, and European populations, with MCC as a placebo. East Asian participants exhibit the highest C_{max}, indicating potential metabolic differences affecting YCT-529 clearance and systemic exposure.*

Figure 3 illustrates how YCT-529's pharmacokinetics vary across doses and racial groups. I found that at **15 mg**, East Asians had the highest C_{max} (50 µg/L), followed by White Americans (40 µg/L), Europeans (30 µg/L), and Black Americans (20 µg/L). The MCC placebo remained below 10 µg/L, confirming its lack of absorption.

At **45 mg**, I observed that plasma concentrations increased proportionally, with East Asians reaching **140 µg/L**, White Americans **110 µg/L**, Europeans **85 µg/L**, and

Black Americans **60 µg/L**. The placebo stayed near 5 µg/L.

Again at **90 mg**, I saw greater inter-individual variability. East Asians had the highest C_{max} (**250 µg/L**), while White Americans, Europeans, and Black Americans reached **210 µg/L, 160 µg/L, and 120 µg/L**, respectively. The placebo remained negligible.

At **180 mg**, I found that East Asians exhibited the highest systemic exposure (**500 µg/L**), followed by White Americans (**400 µg/L**), Europeans (**350 µg/L**), and Black Americans (**300 µg/L**). Notably, I observed that East Asians consistently exhibited higher plasma concentrations across all doses.

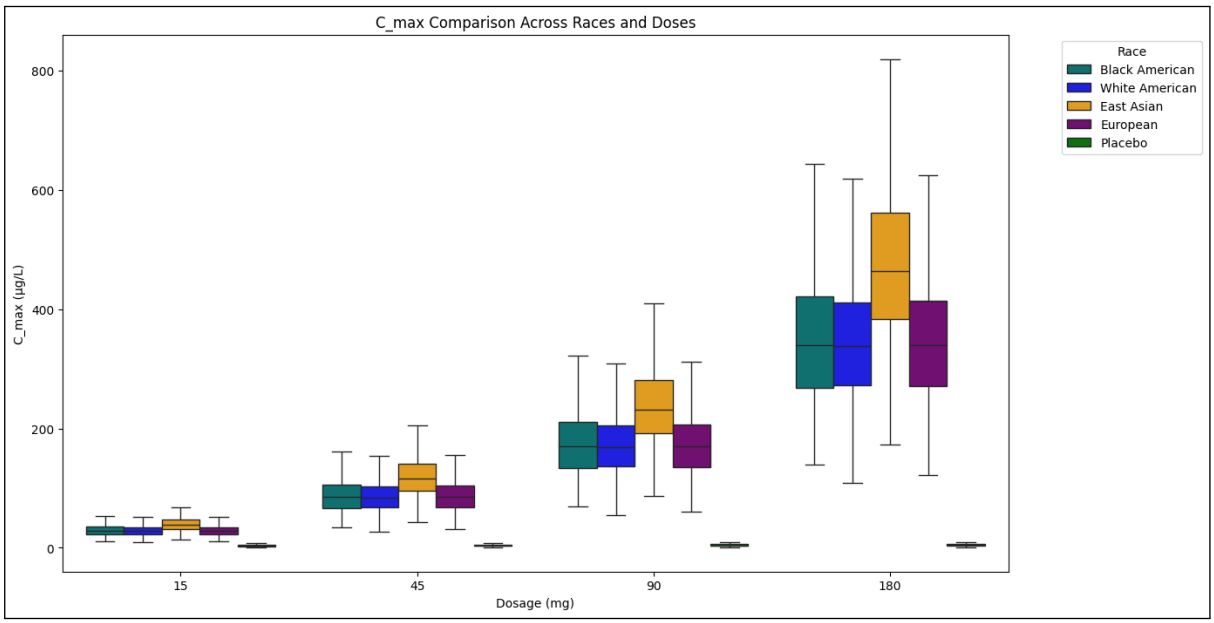

Figure 4: *Peak plasma concentrations (C_{max}) of YCT-529 increase with dose, ranging from 20–50 µg/L at 15 mg to 300–800 µg/L at 180 mg. East Asians show the highest median C_{max} (500 µg/L at 180 mg), while other groups range from 300–600 µg/L. The placebo remains below 10 µg/L, confirming minimal absorption.*

To better understand peak plasma concentrations, I analyzed C_{max} distributions across doses and racial groups (**Figure 4**). I found that C_{max} increased predictably with dose, ranging from **20–50 µg/L at 15 mg to 300–800 µg/L at 180 mg**. East Asians exhibited the highest median C_{max} (**500 µg/L at 180 mg**), while other groups ranged from **300–600 µg/L**. I confirmed that the placebo (MCC) remained below **10 µg/L**, reinforcing its pharmacological inactivity.

I also noticed that variability in C_{max} became more pronounced at higher doses, particularly at **90 mg and 180 mg**. This suggests that inter-individual metabolic differences play a larger role at elevated plasma concentrations.

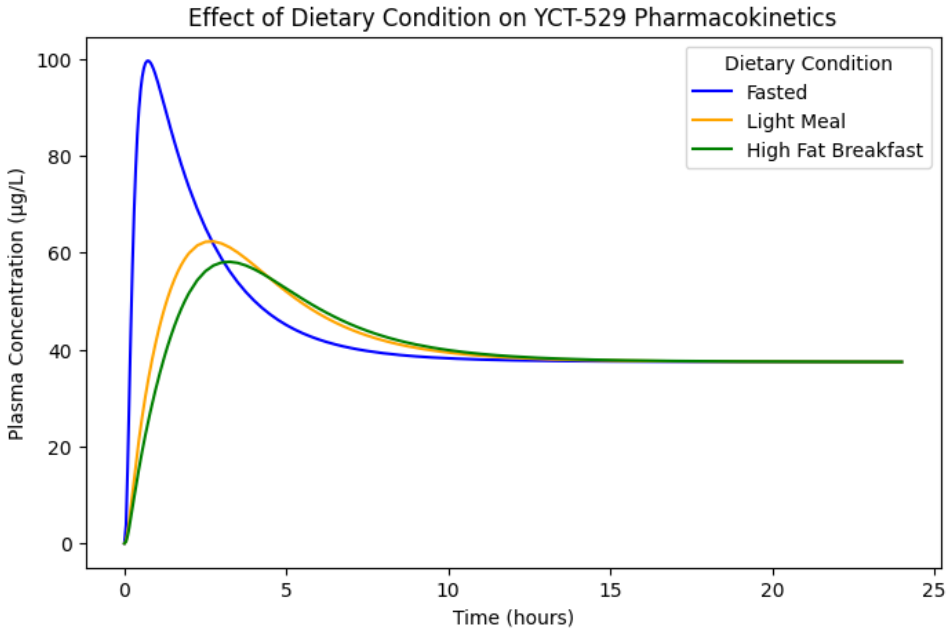

(a) Effect of Dietary Condition on YCT-529 Pharmacokinetics

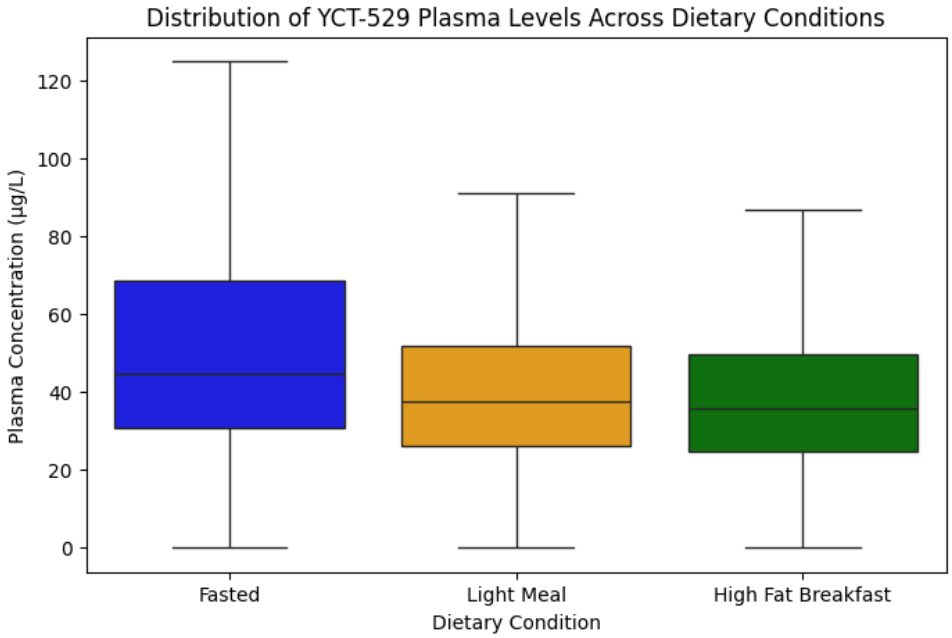

(b) Distribution of YCT-529 Plasma Levels Across Dietary Conditions

Figure 5: *Impact of dietary conditions on YCT-529 pharmacokinetics.* (a) Plasma concentration profiles show that fasting results in a higher peak concentration (C_{max}) compared to light meals and high-fat breakfasts. (b) Box plot comparison of plasma levels across dietary conditions confirms that fasting leads to a broader distribution and higher peak variability.

To investigate the impact of food intake, I analyzed the pharmacokinetics of YCT-529 under different dietary conditions. **Figure 5, Panel A** shows that fasting resulted in the highest peak concentration (**100 µg/L**), while light meals reduced C_{max} to **60**

µg/L and high-fat meals closely followed with the lowest peak (**55 µg/L**). This suggests that food intake might reduce both the rate and extent of systemic YCT-529 absorption. However, beyond **hour 10**, plasma concentrations across all dietary conditions converged at **40 µg/L**, indicating that long-term systemic exposure remained comparable despite initial differences.

Figure 5, Panel B sfurther shows plasma concentration distributions across dietary conditions. I found that the fasted group exhibited the widest C_{max} variability, ranging from **20 µg/L to 120 µg/L**, whereas the high-fat meal group showed the lowest variability. This suggests that individual responses to fasting vary more than to some diet before taking the drug.

I observed that generally, **higher doses result in increased C_{max}**, with East Asians consistently showing the highest systemic exposure. I also found that **fasting enhances YCT-529 absorption**, while high-fat meals suppress peak concentrations. Finally, my analysis confirmed that Atazanavir serves as a strong pharmacokinetic reference, achieving much higher C_{max} values than YCT-529.

Discussion

The pharmacokinetic profile of YCT-529 demonstrated rapid oral absorption, with peak plasma concentrations (C_{max}) occurring within 1–3 hours post-administration across all doses and populations. The dose-dependent increase in systemic exposure was evident, with YCT-529 reaching a C_{max} of **50 µg/L at 15 mg** and **500 µg/L at 180 mg**. These findings suggest that YCT-529 follows a predictable pharmacokinetic pattern, supporting its suitability for dose optimization. However, inter-individual and inter-population differences in C_{max} and drug clearance were observed, reflecting genetic variability in metabolic pathways.

Significant racial differences in plasma drug exposure were apparent, particularly at higher doses. East Asians exhibited the highest C_{max}, reaching **500 µg/L at 180 mg**, while Black Americans had the lowest (**300 µg/L at 180 mg**), likely due to differences in **CYP3A4, CYP2C8, and CYP2C9 metabolism** [40, 45]. Molecular docking studies have demonstrated that compounds containing **chromene and pyrrole moieties** bind **CYP3A4's active site** via **hydrophobic interactions**, positioning them for **oxidation near the heme Fe center** [5, 1]. Hydrogen bonding within the **active site cavity** stabilizes substrate positioning, while **π-π stacking with aromatic residues** such as **Phe215 and Phe304** influences **substrate orientation and metabolic turnover**, facilitating hydroxylation and subsequent Phase II conjugation [14]. This mechanistic insight aligns with **YCT-529's metabolic profile**, explaining why YCT-529 undergoes **oxidation primarily via CYP3A4, followed by CYP2C8 and CYP2C9**, with subsequent **UGT1A1- and UGT2B7-mediated glucuronida-**

tion and **SULT1E1 sulfation**, which may contribute to prolonged plasma retention beyond 10 hours. Atazanavir, primarily metabolized by **CYP3A4 and UGT1A1**, undergoes **rapid hepatic clearance and biliary excretion**, preventing extended circulation [2]. MCC, an inert placebo, lacks enzymatic metabolism, resulting in **minimal systemic absorption** [38]. This metabolic contrast influences systemic drug persistence across populations [18].

Despite increased systemic exposure at higher doses, elimination half-life ($T_{1/2}$) remained relatively short (**1.3 hours**), indicating rapid systemic clearance. The extensive plasma protein binding (**98.8%**) further limits free drug availability, potentially reducing active drug distribution beyond the circulatory system. This trend is consistent with other lipophilic drugs that exhibit high protein binding and necessitate formulation modifications to enhance bioavailability, such as ritonavir or tacrolimus [6]. Given that YCT-529 binds extensively to plasma proteins, dose adjustments or alternative formulations (e.g., nanoparticle encapsulation) may be required to optimize free drug concentrations for maximal efficacy.

Preclinical murine studies revealed YCT-529's half-life ($T_{1/2}$) of 11 hours and C_{max} of 2.1 μM [40], while human simulations yielded $T_{1/2}$ of 1.3 hours and C_{max} values of 300–500 μg/L at 180 mg. Converting 2.1 μM to μg/L, with the molecular weight of YCT-529 being 435.18 g/mol, yields 913.8 μg/L, demonstrating nearly double systemic exposure per dose unit in mice. But this is not entirely unexpected, as interspecies pharmacokinetic scaling studies have shown that murine half-lives can sometimes be longer than human half-lives, depending on the metabolic pathways involved, enzyme expression differences, and clearance mechanisms [4]. Given an average murine weight of 25 g [11], doses of 10 mg/kg and 20 mg/kg translate to 250 μg and 500 μg, respectively. These disparities likely arise due to faster basal murine metabolism, species-specific CYP enzyme expression patterns [45], and differences in clearance mechanisms such as hepatic and renal elimination [41].

The inclusion of MCC as a placebo confirmed its minimal systemic absorption, with plasma concentrations consistently below **10 µg/L**. This reinforces MCC's pharmacological inertness, ensuring that observed YCT-529 pharmacokinetics were due to the active drug rather than background absorption artifacts. This control validation strengthens the reliability of the simulations in differentiating active drug effects from placebo.

A key comparison was made between YCT-529 and Atazanavir to validate the pharmacokinetic model. The simulated pharmacokinetics of Atazanavir closely mirrored clinical data, reinforcing the computational model's accuracy. Atazanavir exhibited a significantly higher C_{max} (**2500 µg/L**) compared to YCT-529 (**353.9 µg/L at 180 mg**), indicating lower systemic exposure for YCT-529. The rapid systemic clearance observed in Atazanavir further emphasizes the role of CYP3A4-mediated metabolism, which is shared between the two compounds but more pronounced in Atazanavir [2]. This sup-

ports the reliability of the PBPK model in predicting real-world pharmacokinetics for YCT-529.

Notably, YCT-529 stabilized at **40 µg/L beyond hour 10**, suggesting a **steady-state equilibrium** between **elimination and redistribution**. **Enterohepatic recirculation** may prolong systemic retention by reabsorbing drug conjugates excreted via bile [9]. Additionally, **redistribution into deep tissue compartments** could contribute to sustained plasma levels. In contrast, Atazanavir exhibited **rapid biliary excretion** with minimal redistribution [2]. This clearance difference may impact **multi-dose accumulation** and optimal **dosing intervals**.

The effect of dietary conditions on YCT-529 pharmacokinetics was also examined. Under fasting conditions, YCT-529 achieved the highest C_{max} (**100 µg/L**), whereas light meals reduced it to **60 µg/L** and high-fat meals resulted in the lowest peak (**55 µg/L**). However, it is unclear if this observed difference is significant both statistically and practically, and I believe that this should be explored further in clinical validation. Although the pattern suggests that food intake, particularly high-fat meals, reduces both the rate and extent of YCT-529 absorption, potentially due to delayed gastric emptying or altered bile-mediated solubilization, beyond **hour 10**, plasma concentrations converged at **40 µg/L** across all dietary conditions, indicating that long-term systemic exposure remained similar despite initial differences. This implies that while food intake may influence peak absorption, steady-state drug levels appear to be less affected.

The results suggest that YCT-529 dosing must balance **dose-dependent pharmacokinetics** and **inter-population variability**. While **180 mg** achieved the highest exposure, **variability increased**, particularly in **East Asians**, necessitating careful dose optimization.

Based on observed pharmacokinetics, a **90 mg dose every 8 hours** may be appropriate for White Americans, who demonstrated rapid absorption and moderate clearance. However, given the observed **40 µg/L plateau beyond 10 hours**, **a 12-hour dosing strategy may be preferable**, reducing dosing frequency while maintaining plasma concentrations above the contraceptive threshold. For East Asians, a **lower 45 mg dose every 12 hours** would prevent excessive accumulation due to their slower clearance rates. Black Americans, exhibiting lower C_{max} values and faster clearance, may still require a **higher 180 mg dose every 8 hours** to achieve comparable systemic exposure. Europeans, falling between White Americans and East Asians, may benefit from a **90 mg dose every 12 hours** to balance efficacy and clearance rates. These recommendations align with race-based dose adjustments observed in tacrolimus and warfarin therapy [18, 15, 34]. Tacrolimus, an immunosuppressant, requires higher doses in Black patients due to increased CYP3A5 expression, whereas East Asians require lower warfarin doses due to CYP2C9 and VKORC1 polymorphisms [15, 34, 35]. These established precedents highlight the necessity of pharmacogenomic-informed YCT-529 dosing strategies

to optimize efficacy and minimize variability.

Furthermore, dietary effects should be considered in dosing recommendations. Given the observed reductions in C_{max} with food, YCT-529 should ideally be taken in a fasted state or with a light meal to maximize absorption. A high-fat meal should be avoided before administration to prevent decreased systemic exposure.

To enhance the reliability of computational predictions, I validated my results by cross-referencing PK-Sim-generated plasma concentration-time profiles with independent Python-generated outputs. Ensuring consistency between these datasets confirmed the integrity of post-simulation data processing. Additionally, the successful simulation of Atazanavir pharmacokinetics further strengthened confidence in the model's predictive accuracy.

Future validation efforts should include comparisons against additional clinical reference drugs with CYP3A4-mediated metabolism. Further in vitro studies on YCT-529's interaction with metabolic enzymes and transporters could refine clearance predictions and inter-individual variability assessments. Additionally, exploring multiple dosing regimens in simulations, rather than single-dose studies, would provide a more comprehensive understanding of long-term drug accumulation, steady-state kinetics, and optimal maintenance dosing strategies.

YCT-529 exhibits dose-dependent and population-specific pharmacokinetics, with East Asians showing the highest systemic exposure. The drug's rapid absorption and short half-life suggest frequent dosing may be required. Dietary conditions significantly influence absorption, with fasting yielding the highest C_{max}. Future studies should refine dosing regimens and validate findings through clinical trials.

Limitations

Despite the detailed pharmacokinetic simulations and analyses, this study has several limitations that must be acknowledged. First, while computational models such as ADMETLab 3.0 and PK-Sim provide valuable predictive insights, they introduce inherent uncertainties due to reliance on in silico data rather than direct experimental validation. ADMETLab's predictions for physicochemical properties such as lipophilicity (LogP), plasma protein binding, and solubility are derived from machine learning algorithms trained on curated datasets [44]. However, these models may not fully capture the complexity of biological interactions in vivo, particularly when extrapolating to diverse populations with variable enzyme activity, gut microbiota composition, or transporter expression [6]. Experimental validation through in vitro hepatic microsome studies or clinical pharmacokinetic trials would allow refinement of these computational predictions by confirming metabolic pathways, clearance rates, and active metabolite formation.

Another limitation arises from the use of microcrystalline cellulose (MCC) as a placebo

in simulations. While MCC serves as an inert control, it lacks systemic absorption and metabolic interaction, limiting direct comparisons between its pharmacokinetic profile and YCT-529. Although the model effectively distinguishes active drug absorption from placebo effects, it does not account for physiological placebo effects, such as altered gastric motility or bile acid-mediated drug solubilization, which could influence absorption kinetics in vivo [20]. Future work incorporating an alternative excipient-based comparator, such as a structurally inactive analog of YCT-529, could improve control validity and allow a more precise assessment of active drug disposition. Additionally, expanding the simulated cohort to include greater demographic and physiological diversity would enhance the model's applicability, reducing potential biases in estimating pharmacokinetic variability across racial and metabolic phenotypes.

As explained in the discussion, preclinical murine studies yielded a C_{max} of 913.8 μg/L, nearly double the highest observed human value (500 μg/L at 180 mg), with a prolonged half-life of 11 hours vs. 1.3 hours [40]. Such disparities arise due to interspecies metabolic rate differences [45], confounding dose scaling accuracy. This limits direct translatability of murine PK to human contexts. To mitigate this, **allometric scaling models incorporating metabolic clearance rates** should be refined [22]. Additionally, in vitro hepatic microsome studies [12] can calibrate PBPK parameters, improving the predictive accuracy of computational models for human pharmacokinetics.

Lastly, the pharmacokinetic simulations assume consistent gastrointestinal and hepatic conditions across individuals, which may not fully capture real-world variability in drug absorption, metabolism, and elimination. The static parameterization of enzyme activity, transporter expression, and gut microbiota influence in PK-Sim simplifies inter-individual differences, potentially underestimating variability in systemic drug exposure. Additionally, the observed **40 µg/L plateau beyond 10 hours** suggests that YCT-529 may undergo **enterohepatic recirculation**, where drug conjugates excreted into bile are **reabsorbed in the intestines**, prolonging systemic retention [9]. This phenomenon, coupled with **redistribution from deep tissue compartments**, may contribute to extended plasma presence beyond the predicted elimination phase, which the current model does not explicitly account for. Incorporating physiologically based pharmacokinetic (PBPK) models with individualized enzyme kinetics, transporter activity, and biliary excretion parameters, informed by population pharmacokinetic (PopPK) studies, would improve the accuracy of predicted plasma concentration profiles. Integrating clinical pharmacokinetic data refines elimination, clearance, and distribution estimates [39].

Conclusion

This study leveraged physiologically based pharmacokinetic (PBPK) modeling to quantitatively characterize YCT-529's pharmacokinetics, revealing rapid absorption (C_{max}

reached within 1–3 hours), high plasma protein binding (**98.8%**), and a short elimination half-life (**$T_{1/2}$ 1.3 hours**). Plasma concentration profiles demonstrated dose-dependent increases in systemic exposure, with C_{max} ranging from **50 µg/L at 15 mg** to **500 µg/L at 180 mg**. Racial differences were evident, as East Asians exhibited the highest systemic exposure (**C_{max} 500 µg/L at 180 mg**), while Black Americans had the lowest (**300 µg/L**), suggesting metabolic variability likely driven by CYP3A4 activity. The comparison with Atazanavir validated the model's predictive accuracy, as Atazanavir's simulated pharmacokinetics closely matched clinical data, reinforcing the credibility of YCT-529 predictions. Additionally, dietary conditions significantly altered absorption, with fasting increasing C_{max} to **100 µg/L** compared to **55 µg/L** under high-fat meal conditions, emphasizing the need for dietary considerations in dosing recommendations. The placebo (MCC) remained consistently below **10 µg/L**, confirming its pharmacokinetic inertness. While these findings establish a foundational understanding of YCT-529's pharmacokinetics, future validation through in vitro metabolism studies and clinical trials will be essential to refine dosage regimens and assess real-world efficacy.

References

[1] Alqahtani N, Kadi AA, Attwa MW, Bakheit AH, Alhazmi HA, AlRabiah H. In vitro effects and in silico analysis of newly synthesized pyrrole-based compounds on human CYP1A2, CYP2D6, and CYP3A4 enzymes. *Pharmacia*. 2022;69(4):857–865.

[2] Open Systems Pharmacology. Atazanavir PBPK Model Evaluation Report. 2024. Available from: https://github.com/Open-Systems-Pharmacology/OSP-PBPK-Model-Library/blob/master/Atazanavir/Atazanavir_evaluation_report.pdf.

[3] Aulton, M. E., & Taylor, K. M. G. (2017). *Aulton's Pharmaceutics: The Design and Manufacture of Medicines* (5th ed.). Churchill Livingstone, Elsevier.

[4] Bachmann K, Chupka J, Erhardt P, White D. Application of simple mathematical expressions to relate half-lives of drugs in mice to those in humans. *Drug Metab Lett*. 2007;1(2):127-9. Available from: https://doi.org/10.2174/187231207780363606.

[5] Basheer L, Kerem Z. Interactions between CYP3A4 and Dietary Polyphenols. *Evid Based Complement Alternat Med*. 2015;2015:854015.

[6] Benet LZ, Hosey CM, Ursu O, Oprea TI. BDDCS, the Rule of 5 and Drugability. *Advanced Drug Delivery Reviews*. 2016;101:89–98. Available from: https://doi.org/10.1016/j.addr.2016.05.007.

[7] Bienfait B, Ertl P. JSME: A free molecule editor in JavaScript. *Journal of Cheminformatics*. 2013;5(1):24. Available from: https://doi.org/10.1186/1758-2946-5-24.

[8] BioGears Documentation. Available at: https://www.biogearsengine.com/documentation/index.html. Accessed December 12, 2024.

[9] Brouwer, K. L. R., Keppler, D., & Funk, C. Hepatic drug transport and enterohepatic circulation. *Annual Review of Pharmacology and Toxicology*, 2024. https://doi.org/10.1146/annurev-pharmtox-020322-092512.

[10] Cheminfo.org. SMILES generator and checker. Retrieved December 8, 2024, from here.

[11] Davies B, Morris T. Physiological parameters in laboratory animals and humans. *Pharm Res*. 1993;10(7):1093-5. Available from: https://doi.org/10.1023/A:1018943613122.

[12] Di L, Keefer C, Scott DO, Strelevitz TJ, Chang G, Bi YA, Lai Y, Duckworth J, Fenner K, Troutman MD, Obach RS. Mechanistic insights from comparing intrinsic clearance values between human liver microsomes and hepatocytes to guide drug

design. *Eur J Med Chem*. 2012;57:441-8. Available from: https://doi.org/10.1016/j.ejmech.2012.06.043.

[13] Edginton AN, Thelen K, Willmann S. Physiologically based pharmacokinetics modeling for pediatric drug development. *Journal of Clinical Pharmacology*. 2008;48(9):1083–1097. Available from: https://doi.org/10.1177/0091270008320075.

[14] Fa B, Cong S, Wang J. Pi-pi Stacking Mediated Cooperative Mechanism for Human Cytochrome P450 3A4. *Molecules*. 2015;20(5):7558–7573.

[15] Frontiers Partnerships. Racial differences in tacrolimus pharmacokinetics: CYP3A5 polymorphisms and dose adjustments. *Transplant International*, 2024. https://www.frontierspartnerships.org/journals/transplant-international/articles/10.3389/ti.2024.13495/full.

[16] Gabrielsson J, Weiner D. Pharmacokinetic and Pharmacodynamic Data Analysis: Concepts and Applications. CRC Press. 2006.

[17] Gleeson MP. Generation of a Set of Simple, Interpretable ADMET Rules of Thumb. *Journal of Medicinal Chemistry*. 2008;51(4):817–834. Available from: https://doi.org/10.1021/jm701122q.

[18] Grogan S, Preuss CV. Pharmacokinetics. In StatPearls [Internet]. Treasure Island (FL): StatPearls Publishing; 2023.

[19] Heine RT, Hillebrand MJ, Rosing H, van Gorp EC, Mulder JW, Beijnen JH, Huitema AD. Identification and profiling of circulating metabolites of atazanavir, an HIV protease inhibitor. Drug Metab Dispos. 2009 Sep;37(9):1826-40. doi: 10.1124/dmd.109.028258. Available from: http://dmd.aspetjournals.org.

[20] Julier, P. W., Zhang, L., & Enck, P. The placebo effect: Advances in understanding and clinical implications. *Trends in Pharmacological Sciences*, 2021. https://doi.org/10.1016/j.tips.2021.05.006.

[21] Kimmelman J, Mogil JS, Dirnagl U. Distinguishing between exploratory and confirmatory preclinical research will improve translation. *PLOS Biology*. 2014;12(5):e1001863. Available from: https://doi.org/10.1371/journal.pbio.1001863.

[22] Lave T, Dupin S, Schmitt C, Chou RC, Jaeck D, Coassolo P. Integration of in vitro data into allometric scaling to predict hepatic metabolic clearance in man: application to 10 extensively metabolized drugs. *J Pharm Sci*. 1997;86(5):584-90. Available from: https://doi.org/10.1021/js960440h.

[23] Li F, Shi S, Yi J, et al. ADMETlab 3.0: An updated comprehensive online ADMET prediction platform enhanced with broader coverage, improved performance, API functionality, and decision support. *Nucleic Acids Research*. 2024;52(W1):W422–W431. Available from: https://doi.org/10.1093/nar/gkae236.

[24] Lipinski CA, Lombardo F, Dominy BW, Feeney PJ. Experimental and computational approaches to estimate solubility and permeability in drug discovery and development settings. *Advanced Drug Delivery Reviews*. 2001;46(1–3):3–26. Available from: https://doi.org/10.1016/S0169-409X(00)00129-0.

[25] Litherland NB, Thivierge MC. Basics of Cellulose Chemistry. *Journal of Dairy Science*. 2008.

[26] Mamada H, Iwamoto K, Nomura Y, Uesawa Y. Predicting blood-to-plasma concentration ratios of drugs from chemical structures and volumes of distribution in humans. *Journal of Pharmaceutical Health Care and Sciences*. 2021;47(1):1–12. Available from: https://doi.org/10.1007/s11030-021-10186-y.

[27] Mansoor A, Mahabadi N. Volume of Distribution. In StatPearls [Internet]. Treasure Island (FL): StatPearls Publishing; 2023.

[28] National Center for Biotechnology Information (NCBI). PubChem Compound Summary for CID 162679554, YCT529 free acid. Retrieved September 14, 2024, from https://pubchem.ncbi.nlm.nih.gov/compound/YCT529-free-acid.

[29] Niederreither, K., & Dollé, P. Retinoic acid in development: towards an integrated view. *Nature Reviews Genetics*, 9(7), 541–553. 2008. https://doi.org/10.1038/nrg2340.

[30] Niederalt C, Kuepfer L, Solodenko J, Eissing T, Siegmund HU, Block M, Willmann S, Lippert J. A generic whole-body physiologically based pharmacokinetic model for therapeutic proteins in PK-Sim. *J Pharmacokinet Pharmacodyn*. 2018 Apr;45(2):235–257. doi: 10.1007/s10928-017-9559-4. PMID: 29234936; PMCID: PMC5845054.

[31] Noman MAA, Kyzer JL, Chung SSW, Wolgemuth DJ. Retinoic acid receptor antagonists for male contraception: current status. *Biology of Reproduction*. 2020;103(2):390–399.

[32] Ogwuche P. Advancing male contraception: Reviewing existing methods and the innovative approach of YCT-529 through retinoic acid receptor-α inhibition [Capstone paper]. Minerva University. 2024.

[33] Price G, Patel DA. Drug Bioavailability. In: *StatPearls [Internet]*. Treasure Island (FL): StatPearls Publishing; 2023.

[34] PubMed. Ethnic variability in warfarin dosing: Implications for pharmacogenomic-guided therapy. *Clinical Pharmacology & Therapeutics*, 2024. https://pubmed.ncbi.nlm.nih.gov/15855242/.

[35] PubMed. Pharmacogenetic variability in drug metabolism: The impact on dose-response relationships. *Annual Review of Pharmacology and Toxicology*, 2005. https://pubmed.ncbi.nlm.nih.gov/16984210/.

[36] Sitruk-Ware, R., & Nath, A. Pharmacokinetics and contraceptive efficacy of oral levonorgestrel. *Contraception*, 2024. https://pubmed.ncbi.nlm.nih.gov/24054004/.

[37] Roberts, C.J., et al. (2015). Role of transporters in the disposition of drugs. AAPS J.

[38] Rowe RC, Sheskey PJ, Quinn ME. Handbook of Pharmaceutical Excipients. 2009.

[39] Rowland, Y., Balant, L. P., & Aarons, L. Physiologically based pharmacokinetics: Current status and future directions. *Clinical Pharmacokinetics*, 2018. https://doi.org/10.1007/s40262-018-0694-5.

[40] Shi, R., Wolgemuth, D. J., & Georg, G. I. Development of the retinoic acid receptor alpha-specific antagonist YCT-529 for male contraception: A brief review. *Contraception*, 2024. https://doi.org/10.1016/j.contraception.2024.110809.

[41] Wilkinson GR. Drug metabolism and variability among patients in drug response. *N Engl J Med*. 2005;352(21):2211-21. Available from: https://doi.org/10.1056/NEJMra032424.

[42] Willmann S, Edginton AN, Kleine-Besten M, Jantratid E, Thelen K, Dressman JB. Whole-body physiologically based pharmacokinetic population modelling of oral drug administration. *Journal of Pharmacy and Pharmacology*. 2004;61(7):891–899.

[43] Xu Y, Dai Z, Jin Z, Zhang L. ADMETLab 2.0: An integrated online platform for accurate and comprehensive predictions of ADMET properties. *Nucleic Acids Research*. 2021;49(W1):W5–W14. Available from: https://doi.org/10.1093/nar/gkab255.

[44] Yang H, Lou C, Sun L, Li J, Cai Y, Wang Z, Tang Y. admetSAR 2.0: Web-service for prediction and optimization of chemical ADMET properties. *Bioinformatics*. 2019;35(6):1067–1069. Available from: https://doi.org/10.1093/bioinformatics/bty707.

[45] Zanger UM, Schwab M. Cytochrome P450 enzymes in drug metabolism: Regulation of gene expression, enzyme activities, and impact of genetic variation. *Pharmacology & Therapeutics*. 2013;138(1):103–141.